SUPPRTING INFORMATION

Homotypic Heterojunction of Metal Oxygen/Sulfide as an Electron Transport Layer for High-Performance Perovskite Solar Cells

Zhipeng Liu[1], Liang Chen[1], Linlin Qiu[3], Yang Lv[1], Zhiqin Su[1], Jian Sun[1], Pingfan Du[1, 2, *]

[1] *College of Textile Science and Engineering, Zhejiang Sci-Tech University, Hangzhou 310018, PR China*

[2] *Key Laboratory of Intelligent Textile and Flexible Interconnection of Zhejiang Province, Zhejiang Sci-Tech University, Hangzhou 310018, PR China*

[3] *College of Textile and Apparel, Quanzhou Normal University, Quanzhou 362000, China*

*Corresponding author. Tel.: fax: +86 571 86843603.

E-mail address: dupf@zstu.edu.cn (P. Du)

Experimental Sections

Materials: $SnCl_4 \cdot 5H_2O$ of 98.0% and thioacetamide (TAA, C_2H_5NS, 99.0%) were provided by Shanghai Macklin Biochemical Co., Ltd. Indium tin oxide (ITO) glass substrates (sheet resistance: 7-9 Ω/sq, thickness: 1.1 mm, transparency: ≥ 89%) with dimensions of 13 mm × 17 mm and conductive glass cleaning fluid were purchased from Advanced Election Technology Co., Ltd. Lead (II) iodide (PbI_2, 99.99%), formamidinium iodide (FAI, 99.5%), methylammonium bromide (MABr, 99.5%), cesium iodide (CsI, 99.99%), 4-tert-butylpyridine (t-BP, 96%), lithium bis(trifluoromethanesulfonyl)imide (Li-TFSI, 99.95%), Tris[4-(1, 1-dimethylethyl)-2-(1H-pyrazol-1-yl)pyridine]cobaltsaltwith1, 1, 1-trifluoro-N-[(trifluoromethyl)sulfonyl]methanesulfonamide (FK209 Co(III) TFSI, 98%), 2, 2′, 7, 7′-Tetrakis(*N*, *N*-di-*p*-methoxyphenylamine)-9, 9′-spirobifluorene (spiro-OMeTAD, 99.5%) and phenyl-C61-butyric acid methyl ester ($PC_{61}BM$, 99%) were purchased from Xi'an Polymer Light Technology Corp. SnO_2 colloidal solution (15% in water) was purchased from Alfa Aesar. Dimethyl formamide (DMF, 99.8%, anhydrous), dimethyl sulfoxide (DMSO, 99.9%, anhydrous), isopropanol (IPA, 99.7%), chlorobenzene (CB, 99.8%, anhydrous), anhydrous ethyl acetate (EA, 99.5%) and acetonitrile (ACN, 99.8%, anhydrous) were supplied by Aladdin. All chemicals were used as received without further purification.

Materials synthesis: The SnS_2 was synthesized using a simple one-step hydrothermal

method. In the synthesis, 2 mmol $SnCl_4 \cdot 5H_2O$ and 8 mmol TAA were added into 25 mL of deionized water with magnetic stirring for 3 h. The slightly yellowed solution was then transferred to a Teflon-lined stainless-steel autoclave and hydrothermally treated at a temperature of 180 ℃ for 16 h. Thereafter, the reaction product was loaded into a centrifuge tube and centrifuged with deionized water and ethanol. After several washing cycles, the prepared SnS_2 powder was then left to dry overnight in a vacuum oven at a temperature of 60 ℃.

Fabrication of SnS_2-SnO_2 ETLs: The colloidal SnO_2 aqueous dispersion solution was diluted to 2.14 wt% using deionized water in order to obtain the precursor of SnO_2. Thereafter, SnS_2 was added into the SnO_2 precursor to obtain a SnS_2-SnO_2 aqueous dispersion solution following stirring at room temperature for 5 h. These precursors (150 μL) were then spin-coated onto pre-cleaned ITO glasses at a rate of 4000 rpm/30 s (2000 rpm/s), followed by thermal annealing at a temperature of 150 ℃ for 30 min in open-air conditions, to obtain the SnO_2 and SnS_2-SnO_2 ETLs.

Perovskite precursor solution: The perovskite precursor was prepared by dissolving PbI_2 (742.2 mg), FAI (224.4 mg), MABr (16.2 mg), and CsI (19.8 mg) into anhydrous DMF/DMSO (v/v: 8:2) to form a mixed solution, which was then stirred at room temperature for 5 h.

Device fabrication: First, the ITO glass substrates were sequentially cleaned for 15 min each in an ultrasonic bath with deionized water with conductive glass cleaning fluid added, acetone and ethanol. The glass substrates were cleaned using IPA through a spin-coating

process at a rate of 5000 rpm for 15 s and then dried in the hot plate at a temperature of 60 °C for 10 min. All the substrates were further treated with UV-ozone for 15 min before the ETL films were deposited. The perovskite films were deposited onto the ETL substrates via a two-step spin-coating process at 1000 rpm/10 s (200 rpm/s) and 5000 rpm/30 s (1000 rpm). After the 70 μL of perovskite precursors were poured onto the substrate dropwise, the 90 μL of antisolvent EA was quickly dropped at the center of the substrate 15 s before the end of the program. The as-prepared perovskite films were then annealed at a temperature of 150 °C for 30 min. Upon being cooled down to room temperature, the HTL precursor solution was prepared by mixing 70 mg of Spiro-OMeTAD powder, 20 μL of t-BP, 70 μL of Li-TFSI solution (170 mg Li-TSFI dissolved in 1 mL ACN), and 50 μL of FK209 Co (III) TFSI Salt (150 mg/mL in ACN) in 1 mL of CB. The obtained HTL precursor solution (40 μL) was then spin-coated on top of the perovskite films at 4000 rpm/30 s (2000 rpm/s). Finally, an Ag electrode grown at a deposition rate of 1.78 nm/s with a thickness of 80 nm with an active area of 0.06 cm^2 was deposited via thermal evaporation. In electron-only device, the $PC_{61}BM$ layer was deposited onto the perovskite film via a spin-coating process at 2000 rpm/30 s (1000 rpm/s) and then annealed at a temperature of 80 °C for 30 min. The $PC_{61}BM$ precursor was prepared by dissolving $PC_{61}BM$ (20 mg) into CB (1 mL). All devices were assembled under ambient conditions with a relative humidity of 25–35% and a temperature ranging from 18–23 °C.

Characterization: Top-view and cross-sectional scanning electron microscopy (SEM) images were characterized through a field-emission scanning electron microscope (FE-

SEM, Ultra 55, Zeiss, Germany) with an electron beam accelerated voltage at 3 kV. Wide-angle XRD measurements were implemented with a Bruker D8 Advance instrument using a Cu Kα source (40 kV, 1.54 Å) with an incidence angle of 1.0°. X-ray photoelectron spectroscopy (XPS, K-Alpha, USA) is performed using a micro-focus monochromatic Al Kα X-ray source, corresponded to the instrument resolution of 0.45 eV. XRD and XPS spectra of ETLs and perovskite films are executed based on the device structure of ITO/SnO_2 (without and with SnS_2 nanosheets). The contact angle of water droplets on surfaces of ITO/SnO_2 (without and with SnS_2 nanosheets) was recorded by a contact angle measurement instrument (Fangrui, Shanghai). Ultraviolet photoelectron spectroscopy (UPS) of the SnO_2 and SnS_2-SnO_2 was carried out by using an ultraviolet photoelectron spectrometer (ESCALAB 250Xi, Thermo Fisher). The UV–Visible absorption and transmission spectra were recorded by a UV–Visible spectrophotometer (UV–Vis, P4, China). The electrochemical impedance spectroscopy (EIS) is measured by a potentiostat (Im6ex/Zahner) to explore charge transfer properties and battery performance with an alternative signal amplitude of 10 mV and a frequency range of 0.01–100 kHz. The steady-state photoluminescence (PL) spectrum PL and Time-resolved PL (TRPL) decay were measured via Fluo Time 300 fluorophotometer Lifetime Spectrometer. Incident photo-to-current conversion efficiency (IPCE) curves are recorded using a quantum efficiency (QE)/IPCE measured system (Solar Cell Scan 100/Zolix) and calibrated by a monocrystalline silicon diode. The photocurrent density−voltage (J–V) characteristics of PSCs were measured with a source meter (2400-SCS, Keithley) under AM1.5 radiation (1

sun conditions, 100 mW cm^{-2}).

Reaction S1. The synthesis mechanism of tin disulfide is as follows:[1]

$$\text{(a) } SnCl_4 \cdot 5H_2O \rightarrow Sn^{4+} + 4Cl^- + 5H_2O$$

$$\text{(b) } CH_3CSNH_2 + 2H_2O \rightarrow CH_3COONH_4 + H_2S$$

$$\text{(c) } Sn^{4+} + 2H_2S \rightarrow SnS_2 + 4H^+$$

$$\text{(d) } Sn^{4+} + 4H_2O \rightarrow Sn(OH)_4 + 4H^+$$

$$\text{(e) } Sn(OH)_4 \rightarrow SnO_2 + 2H_2O$$

$$\text{(f) } SnO_2 + 2H_2S \rightarrow SnS_2 + 2H_2O \qquad \textbf{(S1)}$$

Equation S2. Wenzel equation (Influence of roughness on surface contact angle):

$$\cos\theta^* = \mathrm{r}\cos\theta \qquad \textbf{(S2)}$$

θ^* is the apparent contact angle, θ is the Young's contact Angle, r is Roughness ratio (The ideal smooth appearance is 1)

Equation S3. The electron mobility of ETLs without and with SnS_2 are estimated by the equation:

$$\mu_e = \frac{8JL^3}{9\varepsilon_0\varepsilon(V - V_{bi})^2} \qquad \textbf{(S3)}$$

J is the current density, L is the thickness of ETL, ε_0 is the vacuum permittivity, ε is the relative dielectric constant of ETL.

Equation S4. Gaussian function for peak analysis and peak fitting:

$$y = y_0 + \frac{Ae^{\frac{-4In(2)(x-x_c)^2}{w^2}}}{w\sqrt{\frac{\pi}{4In(2)}}} \quad \textbf{(S4)}$$

y_0 represents the ordinate position of the baseline, A is constant, x_c is the abscissa corresponding to the highest intensity of the diffraction peak, and w represents the half-peak width value (FWHM).

Equation S5. The Debye-Scherrer formula:

$$D = \frac{k\lambda}{w\cos\theta} \quad \textbf{(S5)}$$

D represents the grain size, k is constant, λ is the incidence wavelength of X-rays, θ is the diffraction angle, and w represents the FWHM value.

Equation S6. The PL decay curves are fitted to a bi-exponential decay function:

$$Y = A_1\exp\left(-\frac{t}{\tau_1}\right) + A_2\exp\left(-\frac{t}{\tau_2}\right) + y_0 \quad \textbf{(S6)}$$

A_1 and A_2 are constants representing the contributions of the fast and slow components, respectively. The fast transient component, τ_1, corresponds to the surface characteristics, and the slow component, τ_2, corresponds to the volume characteristics. And y_0 is an offset constant.

Equation S7. The average TRPL lifetime is calculated by the equation:

$$\tau_{ave} = \frac{A_1 * \tau_1^2 + A_2 * \tau_2^2}{A_1 * \tau_1 + A_2 * \tau_2} \quad \textbf{(S7)}$$

Equation S8. The open-circuit voltage dependence on light intensity is fitted using the following equation:

$$V_{oc} = \frac{nkT}{q} In(I) \quad \textbf{(S8)}$$

k is the Boltzmann constant, T is the absolute temperature, q is the elementary charge, I is the light intensity.

Equation S9. The trap density is calculated using the following equation:

$$N_{defects} = \frac{2\varepsilon_0 \varepsilon_r V_{TFL}}{eL^2} \quad \textbf{(S9)}$$

where ε_r is the relative dielectric constant, e is the electron charge, and L is the thickness of the perovskite layer (~ 500 nm).[2,3]

Equation S10. The hysteresis index of the PSCs is calculated by the following equation:

$$Hysteresis\ index = \frac{PCE_{Reverse} - PCE_{Forward}}{PCE_{Reverse}} \times 100\% \quad \textbf{(S10)}$$

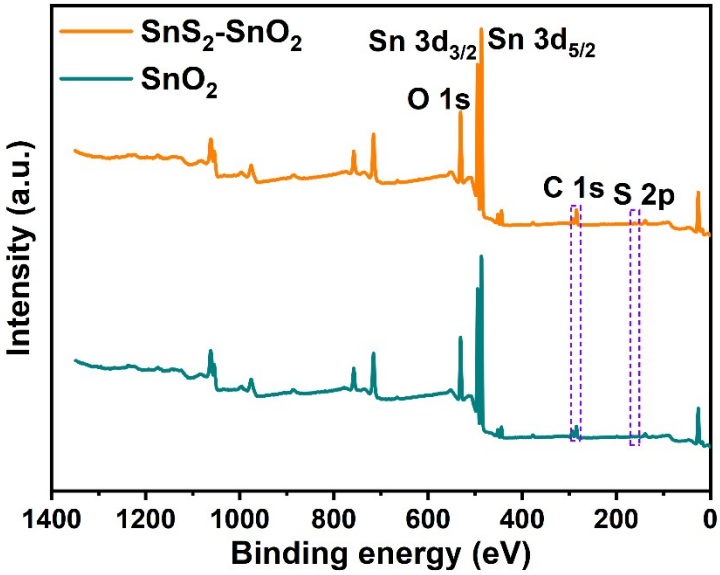

Figure S1. Survey XPS spectra for the SnO_2 and SnS_2-SnO_2 films.

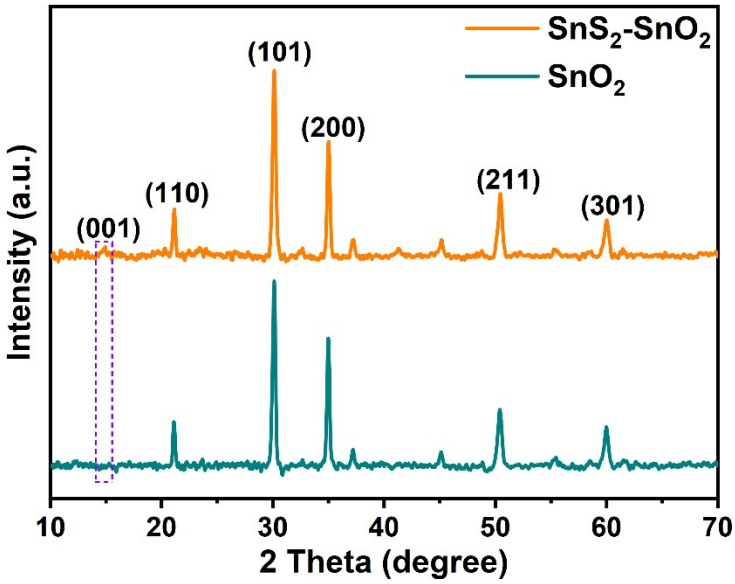

Figure S2. The acquired XRD patterns for the SnO_2 and SnS_2-SnO_2 films.

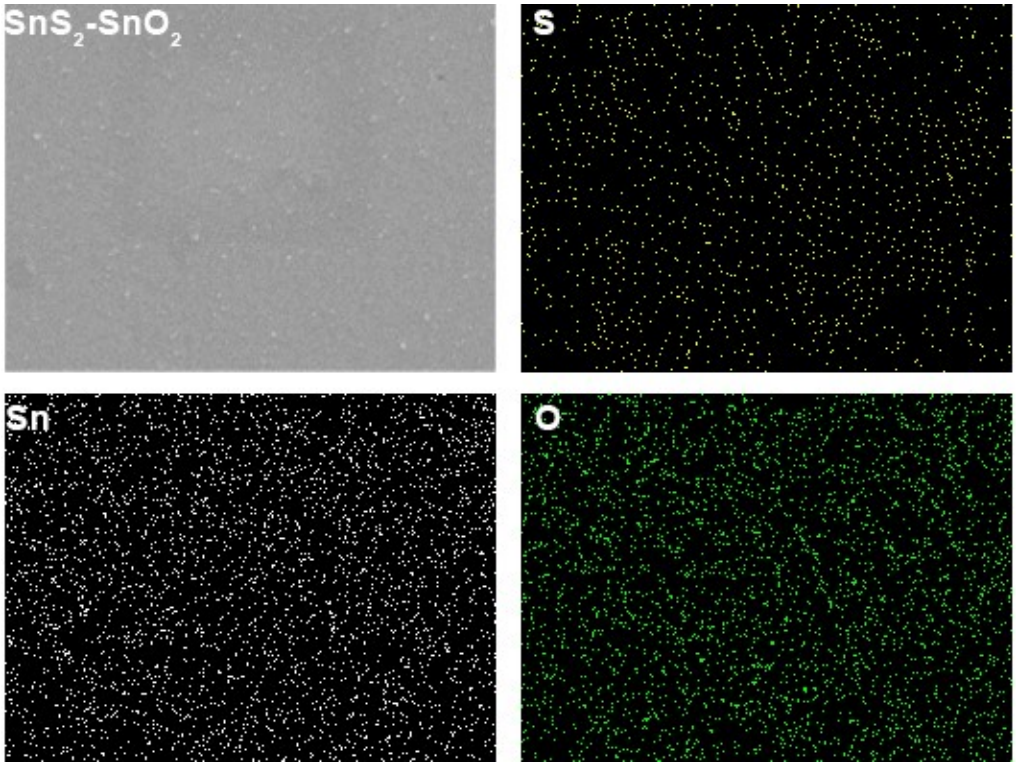

Figure S3. Images obtained from the SEM elemental mapping analysis for the SnS_2-SnO_2 film.

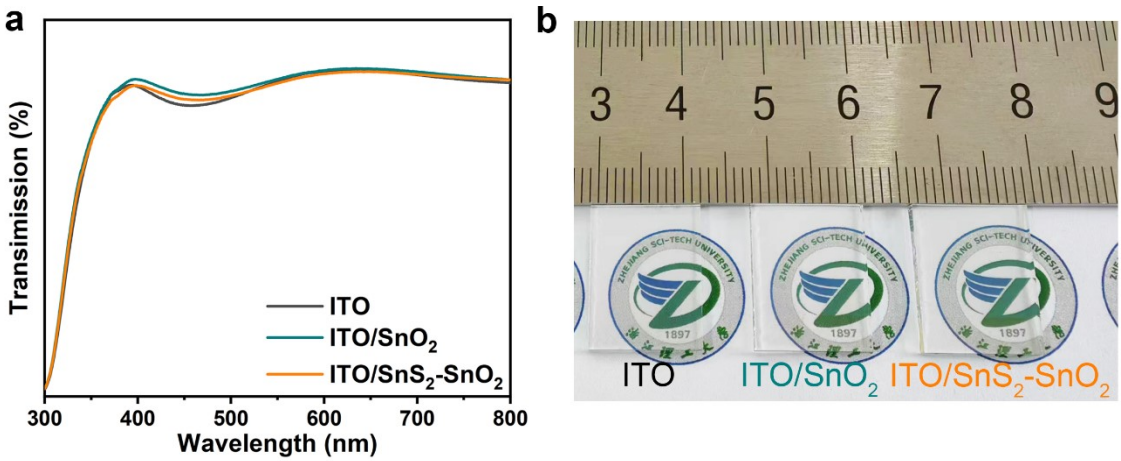

Figure S4. (a) Transmittance spectra and **(b)** photograph of the pristine SnO_2 and SnS_2-SnO_2 films deposited on the glass/ITO substrate.

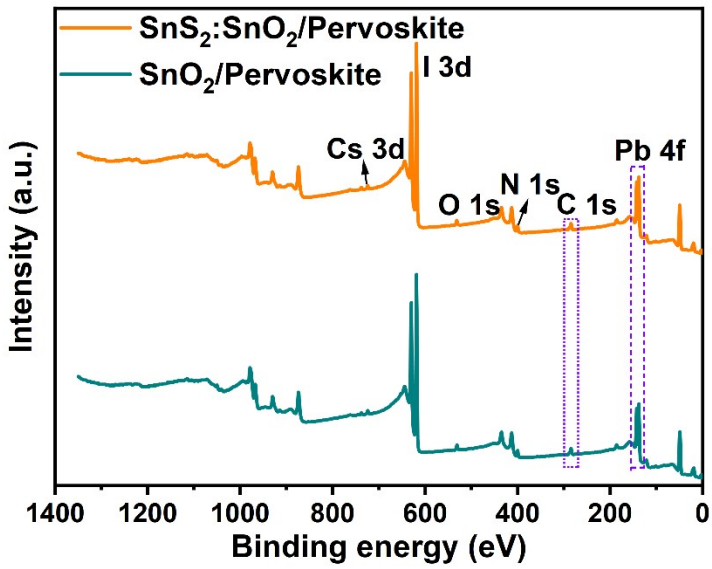

Figure S5. Survey XPS spectra for the perovskite films.

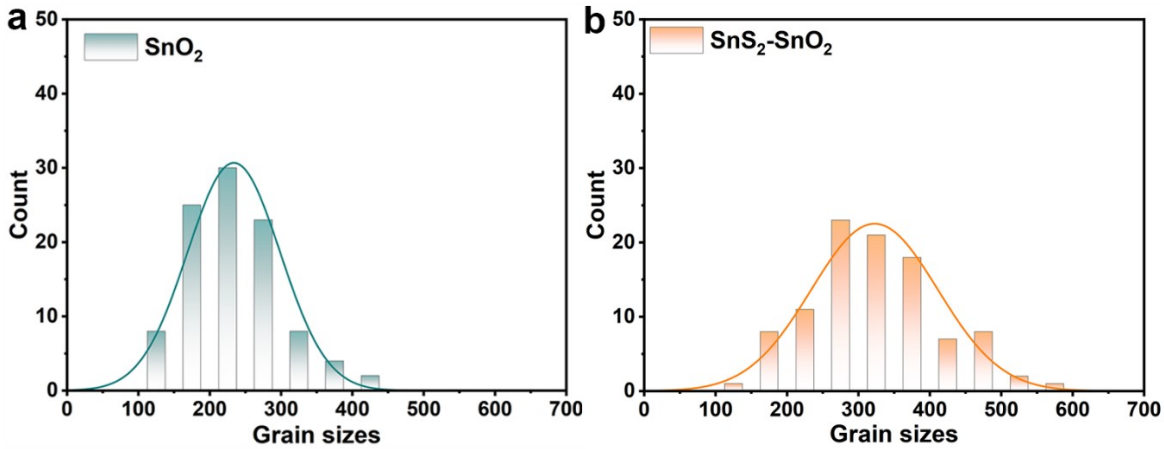

Figure S6. Statistical diagram of the grain size distribution for perovskite layers deposited on the **(a)** SnO_2 and **(b)** SnS_2-SnO_2 films.

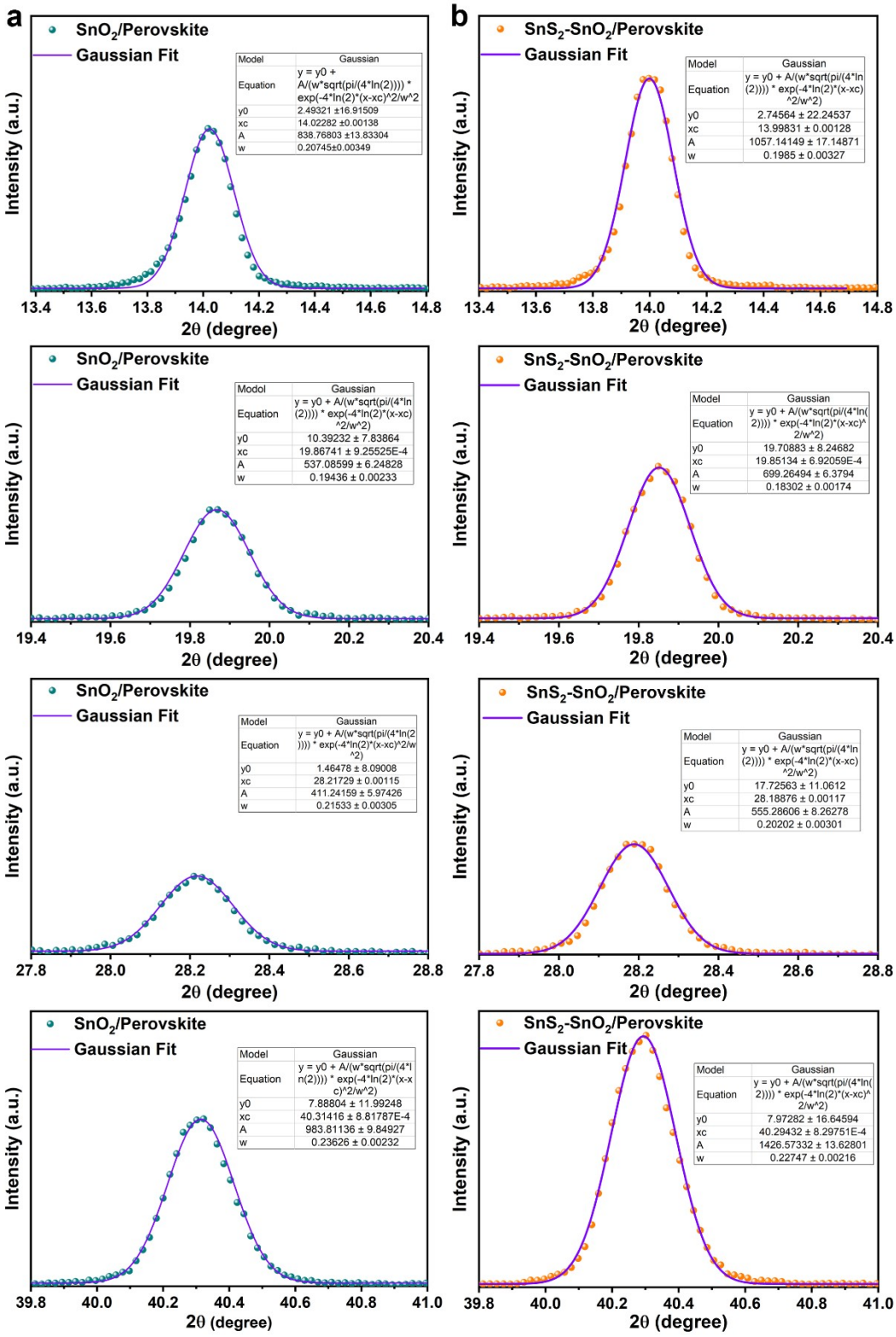

Figure S7. Gaussian fitting curves for the correlative characteristic peaks of the perovskite layer grown on the **(a)** SnO_2 and **(b)** SnS_2-SnO_2 films.

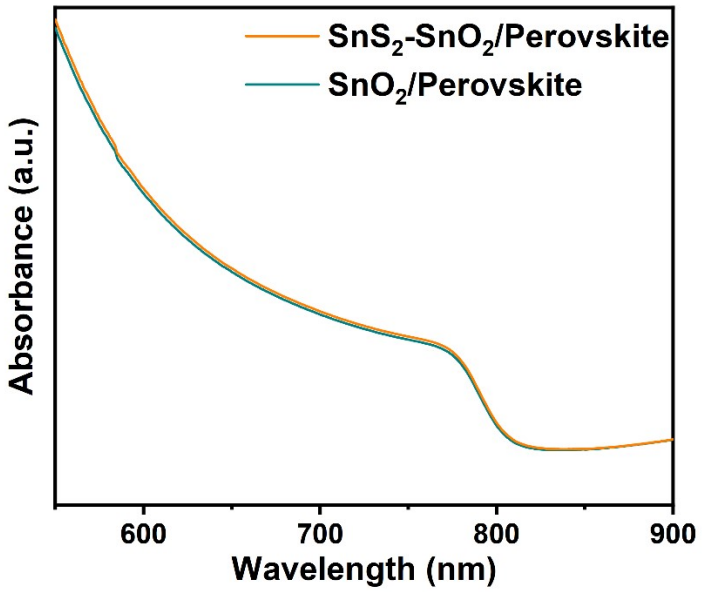

Figure S8. UV-Vis absorbance spectra for perovskite layers deposited on the SnO_2 and SnS_2-SnO_2 films.

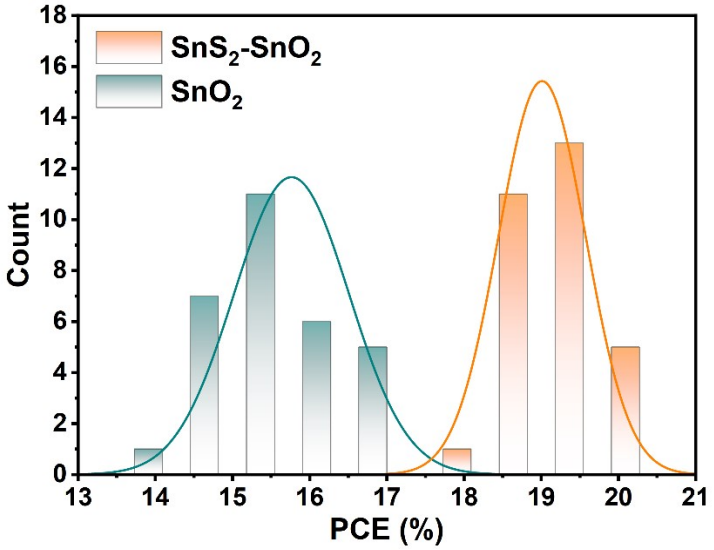

Figure S9. The PCE distribution histogram for the prepared PSC devices based on the SnO_2 and SnS_2-SnO_2 ETLs.

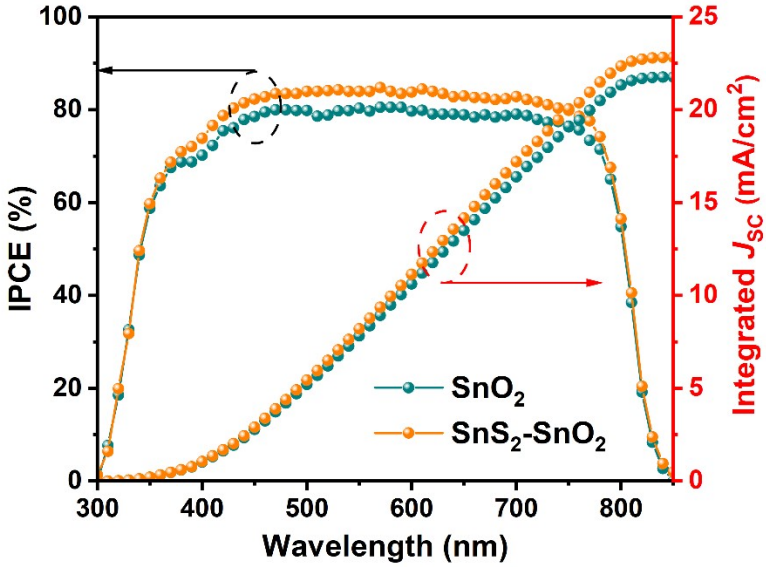

Figure S10. IPCE spectra and integrated J_{SC} values of the devices based on the SnO_2 and SnS_2-SnO_2 ETLs.

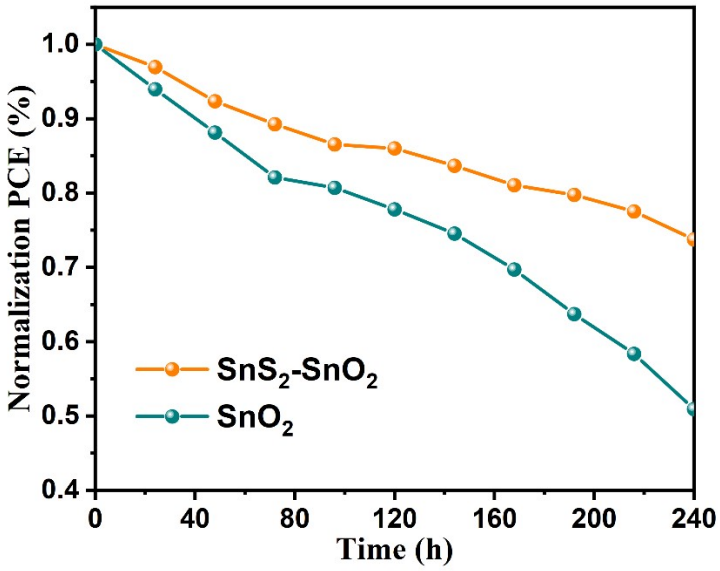

Figure S11. Long-term stability test at 25 ± 5 °C, 75%–85% RH.

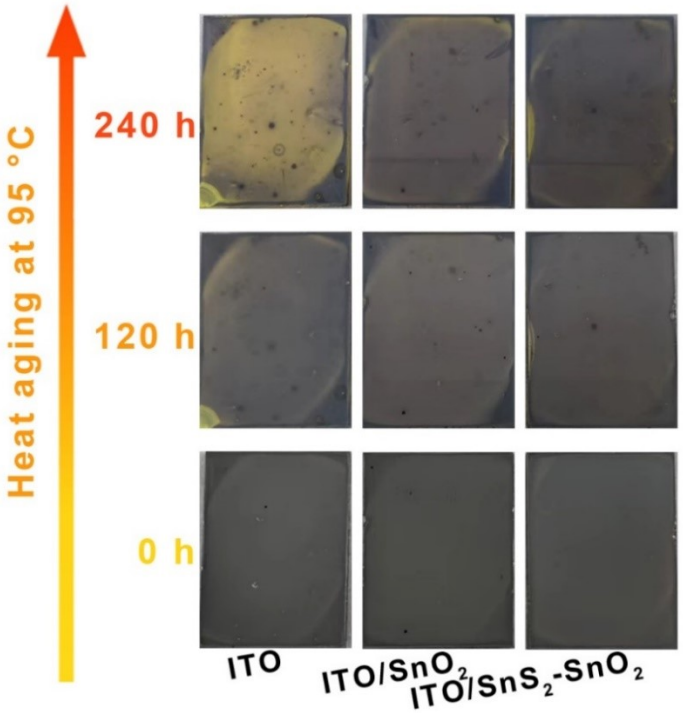

Figure S12. Decay state with thermal aging (~ 40% RH, 95 °C) for the perovskite active layer deposited on different substrates.

Table S1. The detailed calculated UPS parameters for ETLs without and with SnS_2.

ETLs	$E_{cut\text{-}off}$ (eV)	E_{onset} (eV)	W_F (eV)	E_V (eV)	E_g (eV)	E_C (eV)
SnO_2	16.52	3.50	4.70	8.20	3.95	4.25
SnS_2-SnO_2	16.62	3.34	4.60	7.94	3.93	4.01

Table S2. The calculation results of the XRD FWHM of the perovskite deposited on SnO_2 with and without SnS_2, corresponding to Figure 4e and S7.

Sample	2θ	y_0	x_c	A	w *(angle)*
SnO_2/perovskite	14.01°	2.49321	14.02282	838.76803	0.20745
	19.87°	10.39232	19.86741	537.08599	0.19436
	28.21°	1.46478	28.21729	411.24159	0.21533
	40.32°	7.88804	40.31416	983.81136	0.23626
SnS_2-SnO_2/perovskite	14.00°	2.74564	13.99831	1057.14149	0.19850
	19.84°	19.70883	19.85134	699.26494	0.18302
	28.19°	17.72563	28.18876	555.28606	0.20202
	40.30°	7.97282	40.29432	1426.57332	0.22747

Table S3. The fitted data from TRPL curves.

Sample	A_1	τ_1 (ns)	A_2	τ_2 (ns)	τ_{ave} (ns)
SnO_2	0.24286	50.47074	0.66089	158.47397	147.16
SnS_2-SnO_2	0.33621	23.28331	0.70245	79.95196	72.41

Table S4. The fitted values of internal series resistance (R_s) and recombination resistance (R_{rec}) for PSCs based on different ETLs.

Sample	R_s (Ohm)	R_{rec} (Ohm)	*CPE-T* (F)	*CPE-P* (F)
SnO_2	13.49	12915	1.4055E-8	0.97228
SnS_2-SnO_2	7.313	16017	1.8541E-8	0.95400

Table S5. The detailed photovoltaic parameters of the devices based on SnS_2 additive with different concentrations prepared under air conditions. The devices are based on ITO/ SnS_2-SnO_2/perovskite/spiro-OMeTAD/Ag configuration.

Device	Concentrations	J_{SC} (mA cm^{-2})	V_{OC} (V)	*FF* (%)	*PCE* (%)
SnS_2-SnO_2	0 mg/mL	22.48	1.04	71.60	16.74
	1 mg/mL	23.21	1.05	75.62	18.43
	2 mg/mL	23.52	1.08	78.64	19.98
	3 mg/mL	23.25	1.07	77.06	19.17
	4 mg/mL	23.02	1.05	72.11	17.43

Table S6. The detailed photovoltaic parameters of the control devices and the best devices, reverse scan (1.2V → –0.1 V) and forward scan (–0.1 V → 1.2V).

Device		J_{SC} (mA cm^{-2})	V_{OC} (V)	*FF* (%)	*PCE* (%)	*HI* (%)
SnO_2	Reverse	22.48	1.04	71.60	16.74	4.90
	Forward	22.30	1.03	69.31	15.92	
SnS_2-SnO_2	Reverse	23.52	1.08	78.64	19.98	2.40
	Forward	23.34	1.08	77.48	19.53	

1. Y. C. Zhang, L. Yao, G. Zhang, D. D. Dionysiou, J. Li and X. Du, *Applied Catalysis B: Environmental*, 2014, **144**, 730–738.
2. Q. Dong, Y. Fang, Y. Shao, P. Mulligan, J. Qiu, L. Cao and J. Huang, *Science*, 2015, **347**, 967–970.
3. H. Liu, Z. Chen, H. Wang, F. Ye, J. Ma, X. Zheng, P. Gui, L. Xiong, J. Wen and G. Fang, *Journal of materials chemistry A*, 2019, **7**, 10636–10643.